



Geophysical Research Letters

Supporting Information for

Rupture Process during the M_w 8.1 2017 Chiapas Mexico Earthquake: Shallow Intraplate Normal Faulting by Slab Bending

R. Okuwaki¹, and Y. Yagi²

¹Graduate School of Life and Environmental Sciences, University of Tsukuba, 1-1-1 Ten'nodai, Tsukuba, Ibaraki 305-8572, Japan.

²Faculty of Life and Environmental Sciences, University of Tsukuba, 1-1-1 Ten'nodai, Tsukuba, Ibaraki 305-8572, Japan.

Corresponding author: Ryo Okuwaki (rokuwaki@geol.tsukuba.ac.jp)

Contents of this file

Text S1

Figures S1 to S7

Tables S1 to S3

Introduction

This file contains Text S1 describing the centroid moment tensor (CMT) inversion procedure to retrieve the CMT solution shown in Figure 2b, along with all the finite fault models constructed in this study with the variable assumptions of the initial rupture depth, fault geometry, and the near-source velocity structure (Tables S1 to S3) through Figures S1 to S4. Waveform fittings, and the variance the slip models shown in Figure 3 are presented in Figures S5 and S6, respectively. Figure S7 shows the vertical P -wave Green's functions (GFs) and the convolutions of the GFs and a source time function.

Text S1. Centroid moment tensor inversion

We downloaded the 34 globally observed teleseismic P-waveforms in a vertical component through the Incorporated Research Institutions for Seismology Data Management Center (IRIS DMC; Figure 3d). The data were selected to ensure high signal-to-noise ratio to pick the clear first motion of the P-phase, and azimuthal distribution to cover the diverse feature of the radiation pattern of the waveforms. The instrumental response for each waveform was deconvolved to displacement at a sampling rate of 0.2 s. We calculated Green's functions based on the method of Kikuchi and Kanamori (1991) at a computation rate of 0.2 s. One-dimensional, near-source velocity structure was extracted from the one presented in Santoya et al. (2005) (Table S1) to calculate the Haskell propagator matrix in Green's functions. We also used the ak135 model (Kennett et al., 1995) to calculate the travel times, the geometrical spreading factors, and the ray parameters for all the procedures. A Butterworth band pass filter in a range of 0.005–0.02 Hz was adopted to both the observed waveforms and the theoretically calculated Green's functions. We searched both the focal depth and half duration of the triangle source time function that reduce the variance most between the observed and synthetic waveforms.

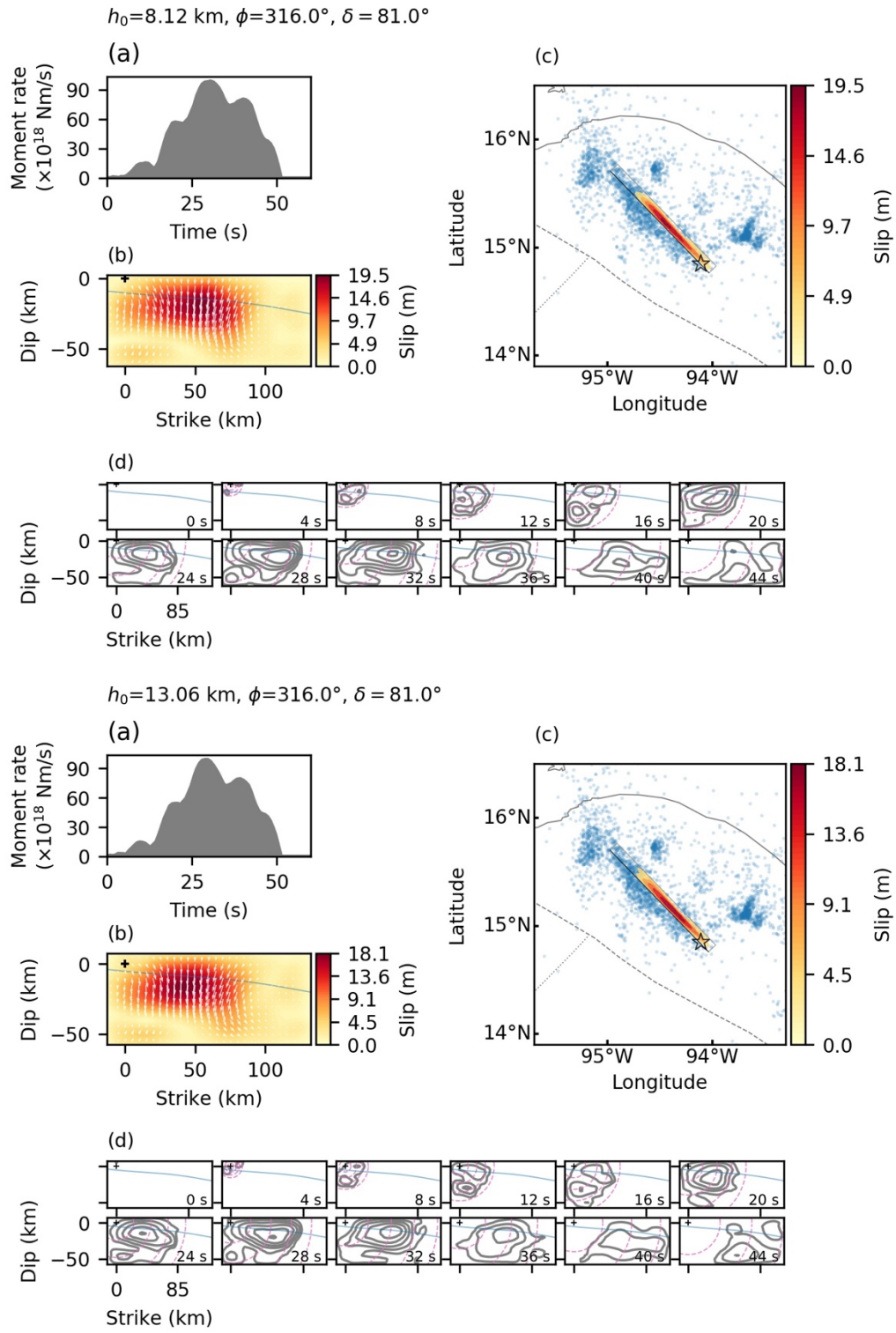


Figure S1. (continued.)

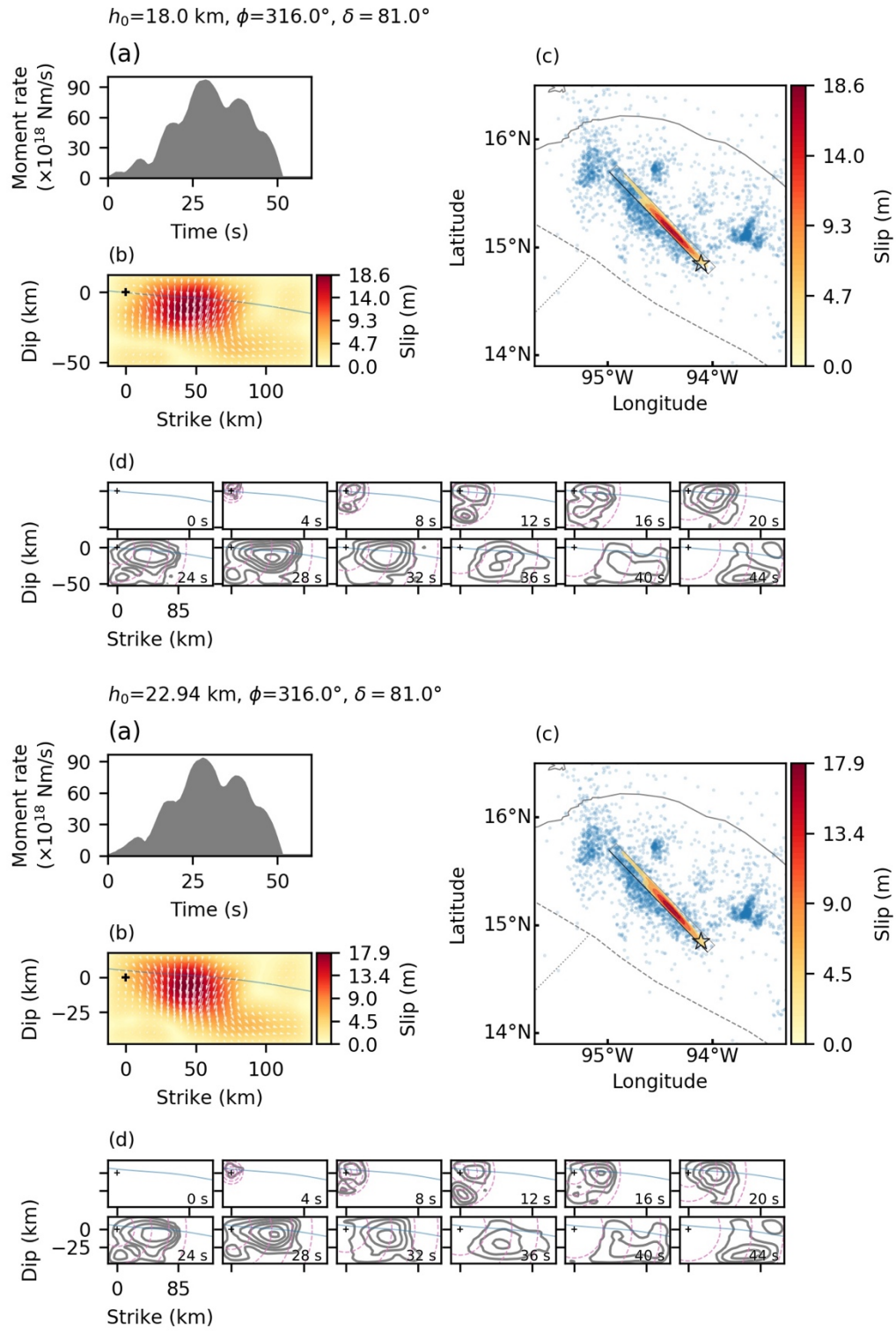


Figure S1. (continued.)

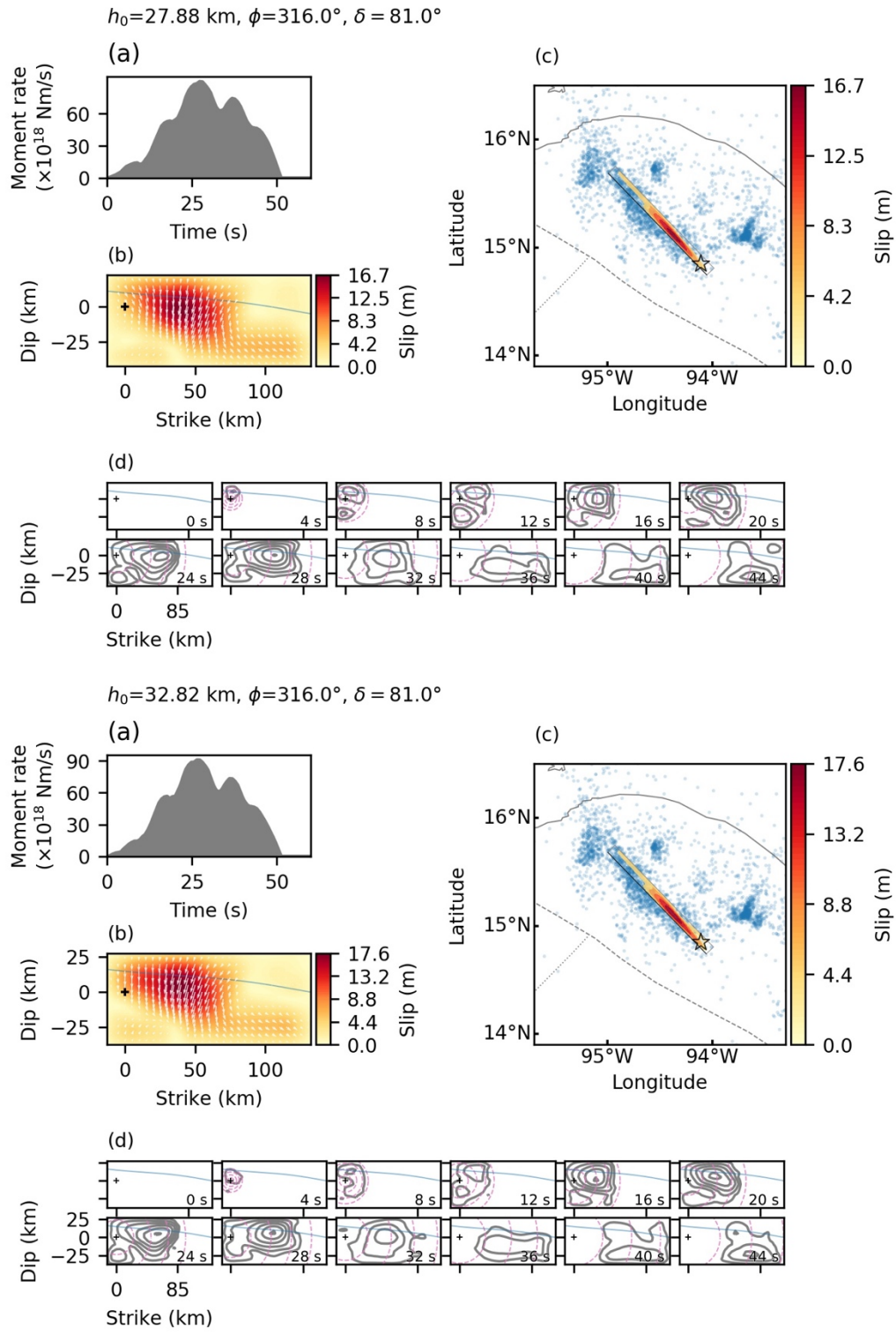


Figure S1. (continued.)

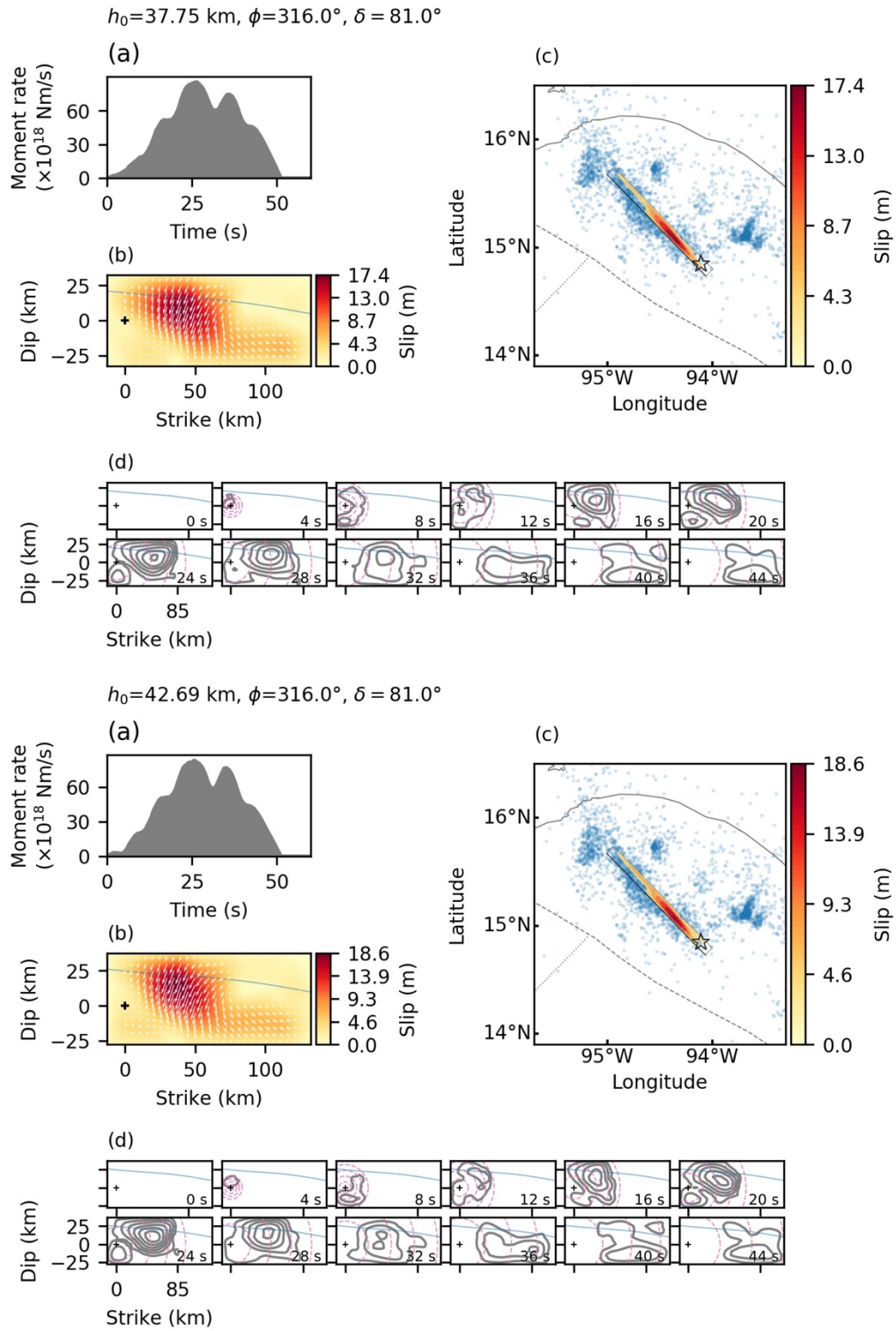


Figure S1. (continued.)

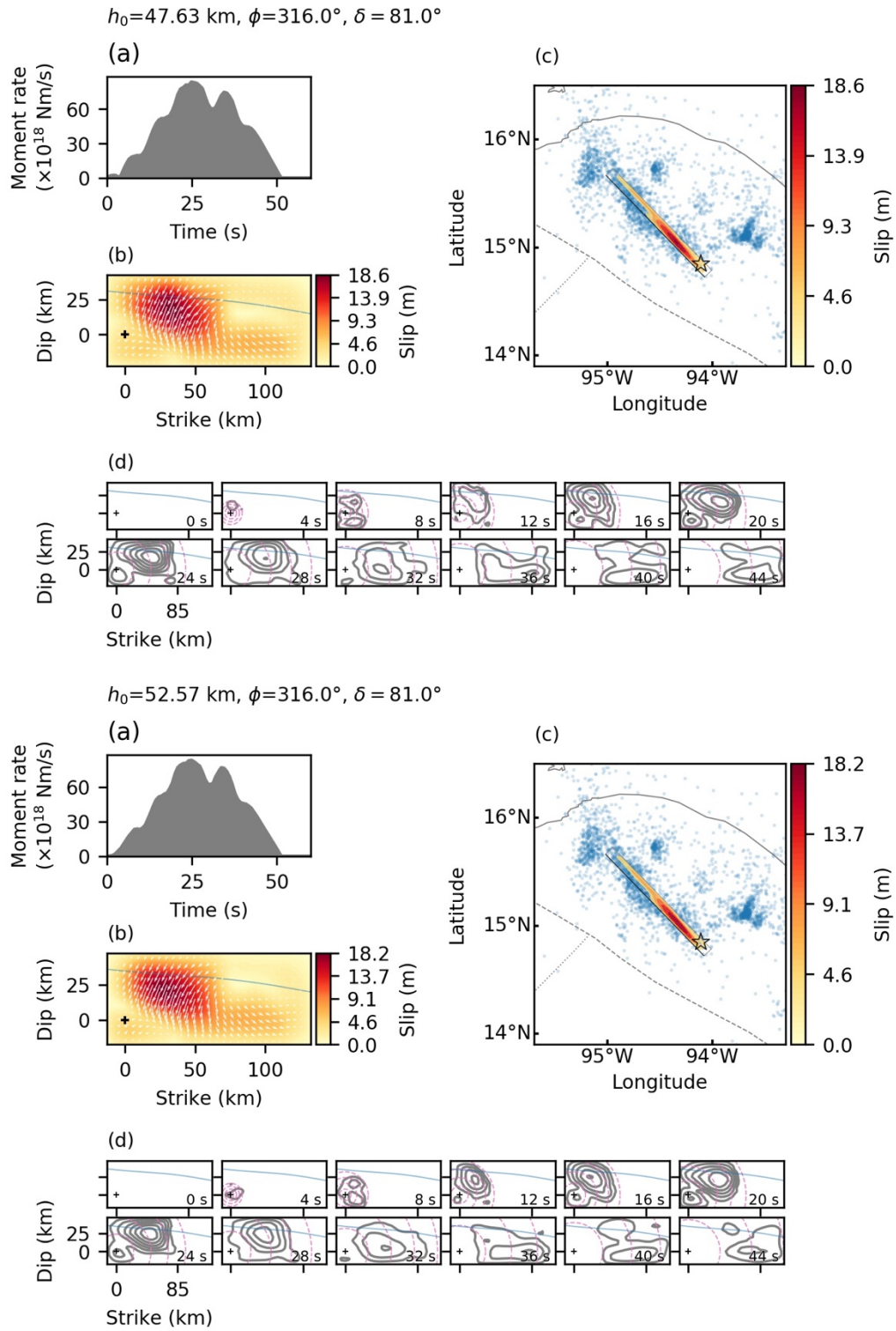


Figure S1. (continued.)

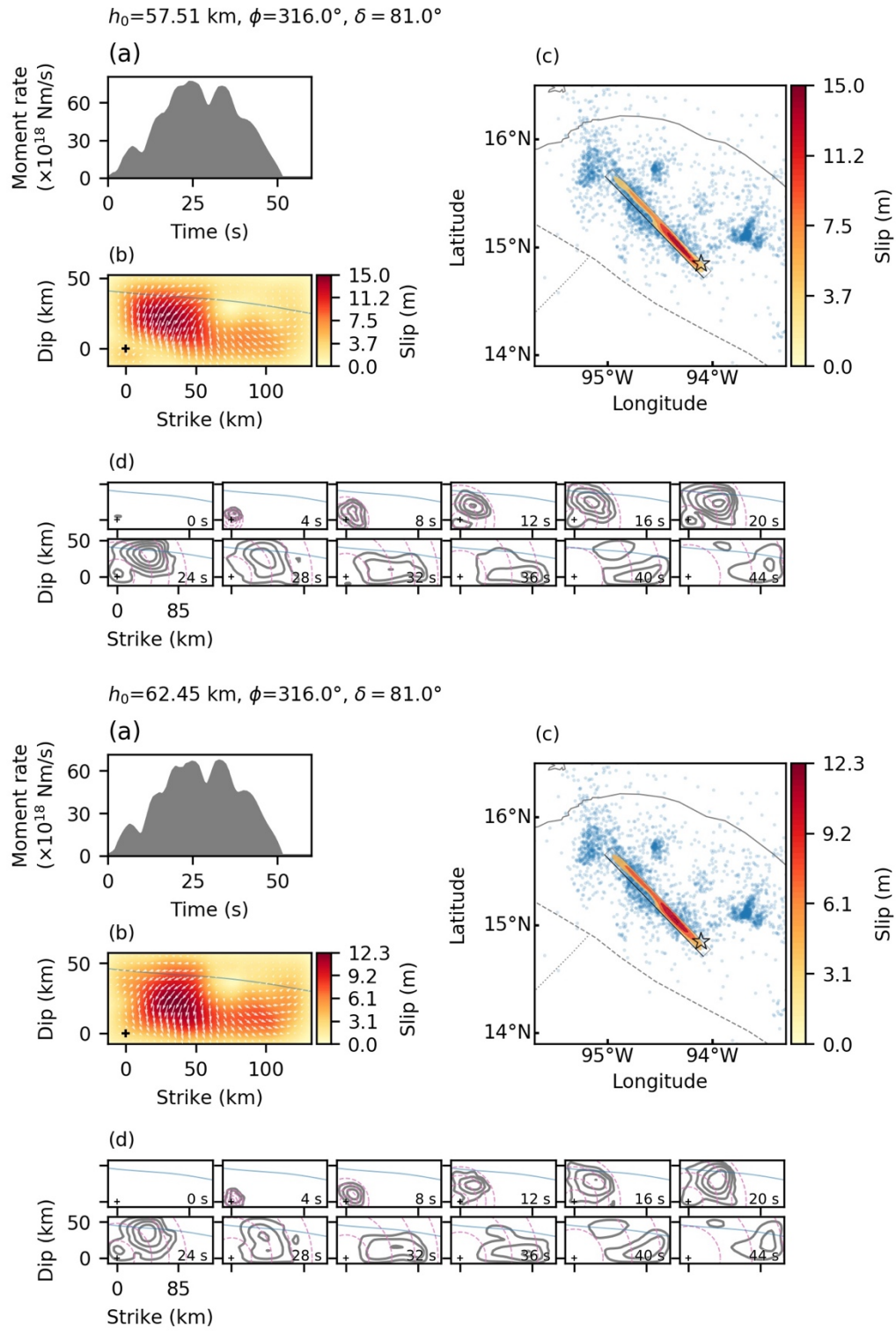


Figure S1. (continued.)

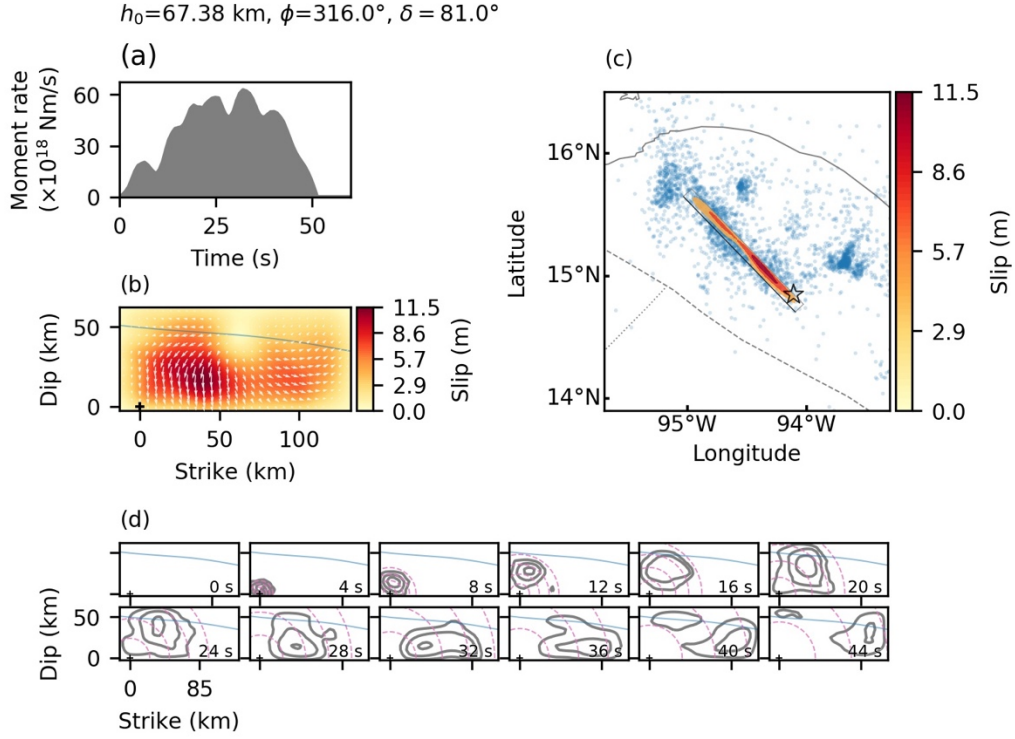


Figure S1. Summary of the slip models with the variable initial rupture depths (8.1–67.38 km) shown in Figure 3. (a) Graph shows the moment-rate function. The initial rupture depth (h_0), strike angle (ϕ), and dip angle (δ) for the assumed fault geometry are given on left top. (b) Cross section of the cumulative slip distribution. The slip amplitude is represented as color map. White arrows represent the slip vectors of the hanging wall relative to the foot wall. The cross marker is the initial rupture point. (c) Map view of the accumulated slip distribution. Color contour denotes every 3.0 m slip. Rectangle delimits the fault plane along with the fault top as black line. Star and blue dots are the epicenters of the mainshock and the two-week-aftershock ($M \geq 3$) determined by the SSN. (d) Snapshots of the slip model taken. The time where the snapshot is taken is denoted at right-bottom on each panel. Gray contour denotes the slip rate every 0.26 m/s. Cross marker shows the initial rupture point, and blue curve represents the Slab1.0 model (Hayes et al., 2012). Pink dashed lines are the reference rupture speeds that constantly expand in a circle at 1, 2, 3, and 4 km/s.

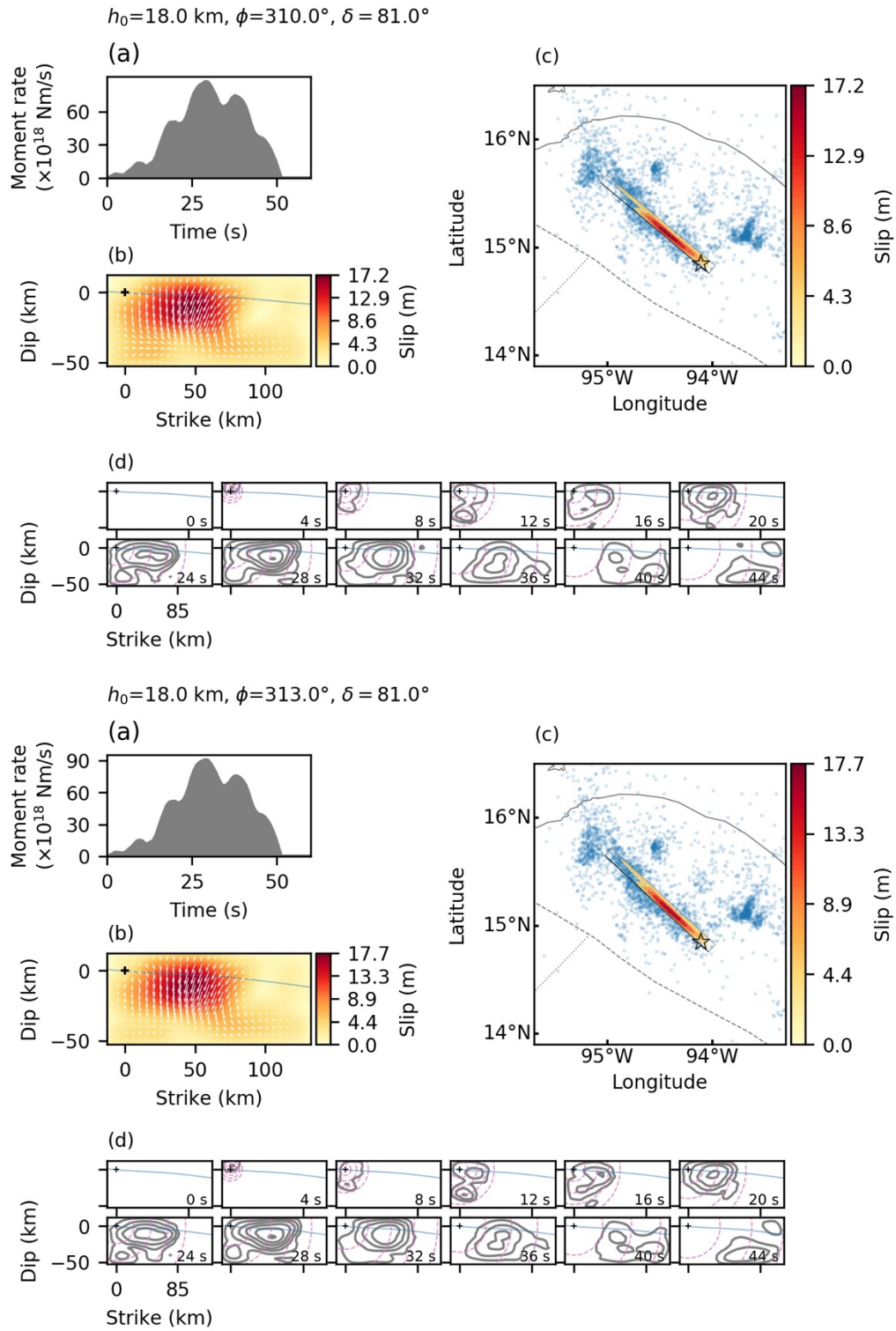


Figure S2. (continued.)

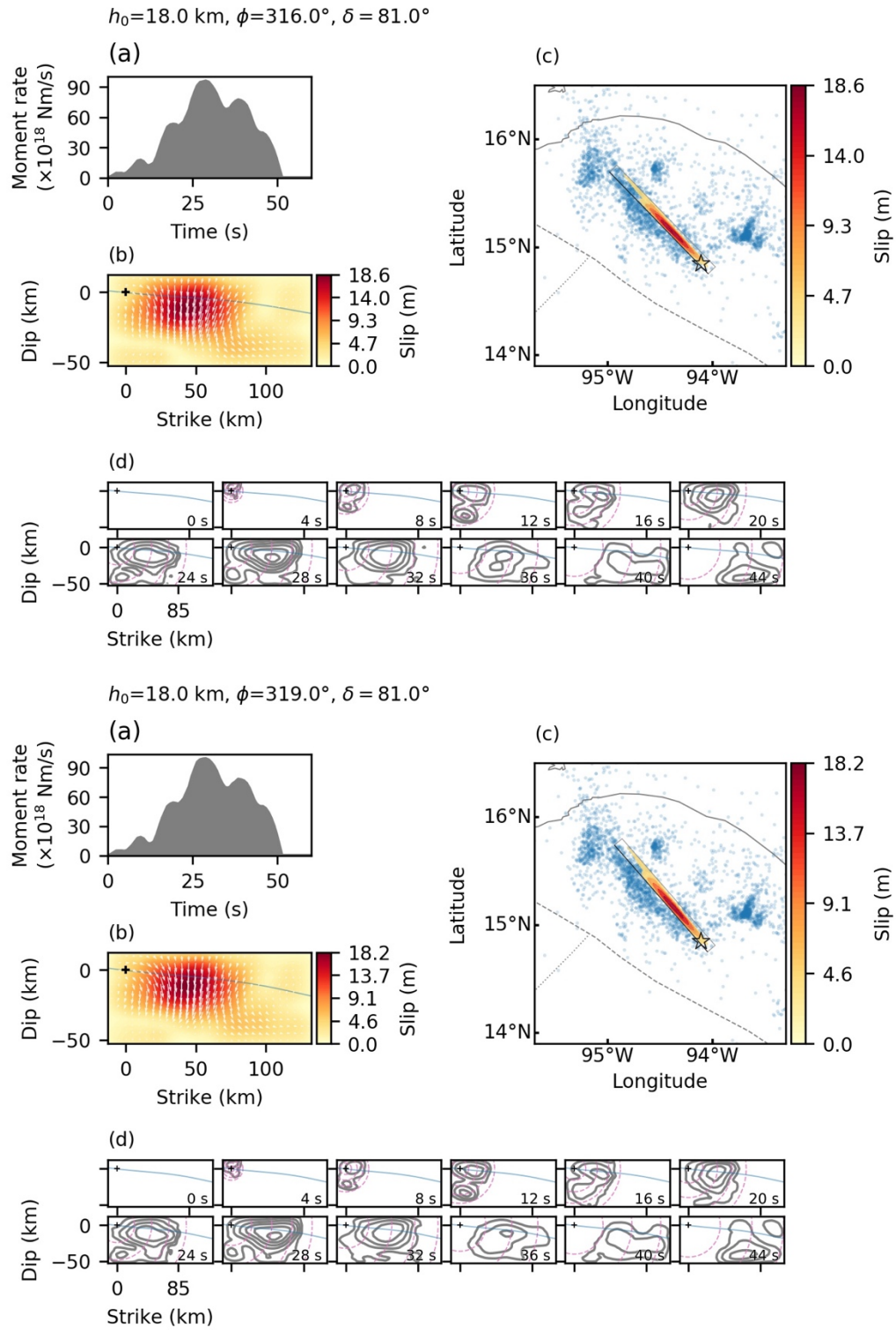


Figure S2. (continued.)

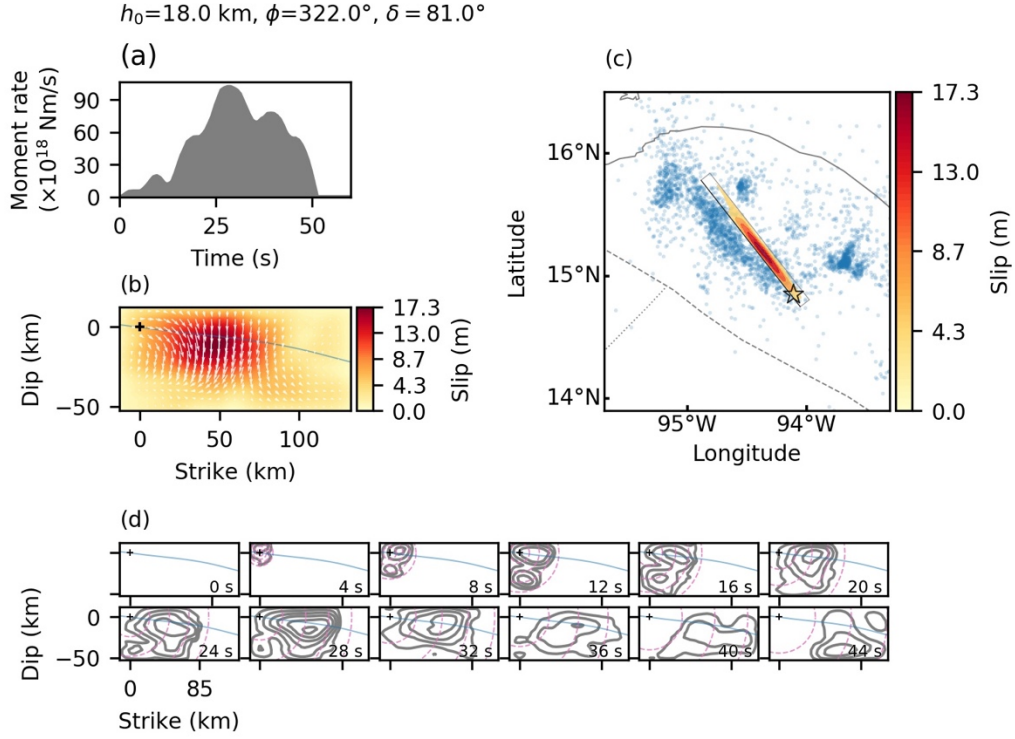


Figure S2. Summary of the slip models with the variable assumptions of strike angle. (a) Graph shows the moment-rate function. The initial rupture depth (h_0), strike angle (ϕ), and dip angle (δ) for the assumed fault geometry are given on left top. (b) Cross section of the cumulative slip distribution. The slip amplitude is represented as color map. White arrows represent the slip vectors of the hanging wall relative to the foot wall. The cross marker is the initial rupture point. (c) Map view of the accumulated slip distribution. Color contour denotes every 3.0 m slip. Rectangle delimits the fault plane along with the fault top as black line. Star and blue dots are the epicenters of the mainshock and the two-week-aftershock ($M \geq 3$) determined by the SSN. (d) Snapshots of the slip model taken. The time where the snapshot is taken is denoted at right-bottom on each panel. Gray contour denotes the slip rate every 0.26 m/s. Cross marker shows the initial rupture point, and blue curve represents the Slab1.0 model (Hayes et al., 2012). Pink dashed lines are the reference rupture speeds that constantly expand in a circle at 1, 2, 3, and 4 km/s.

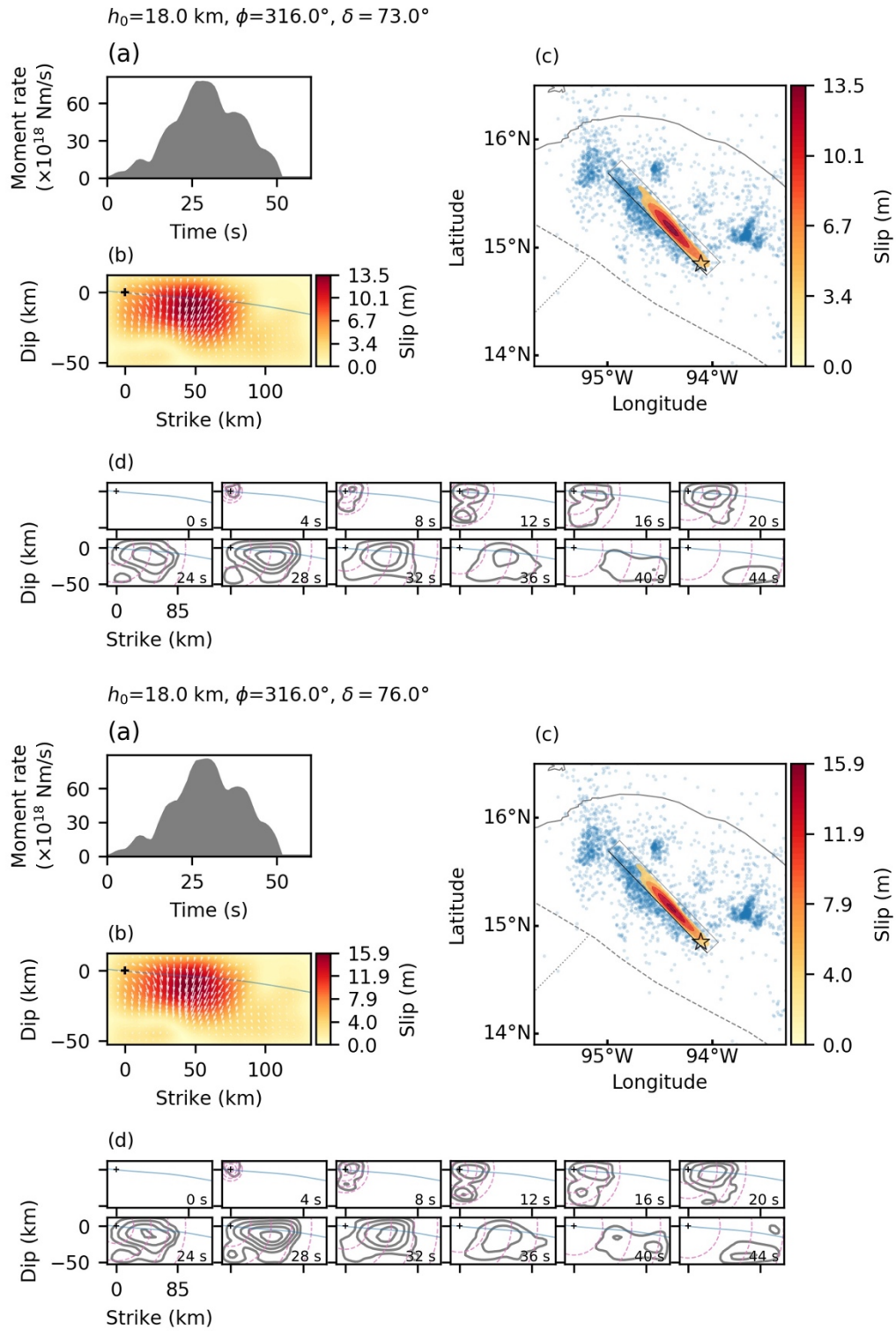


Figure S3. (continued.)

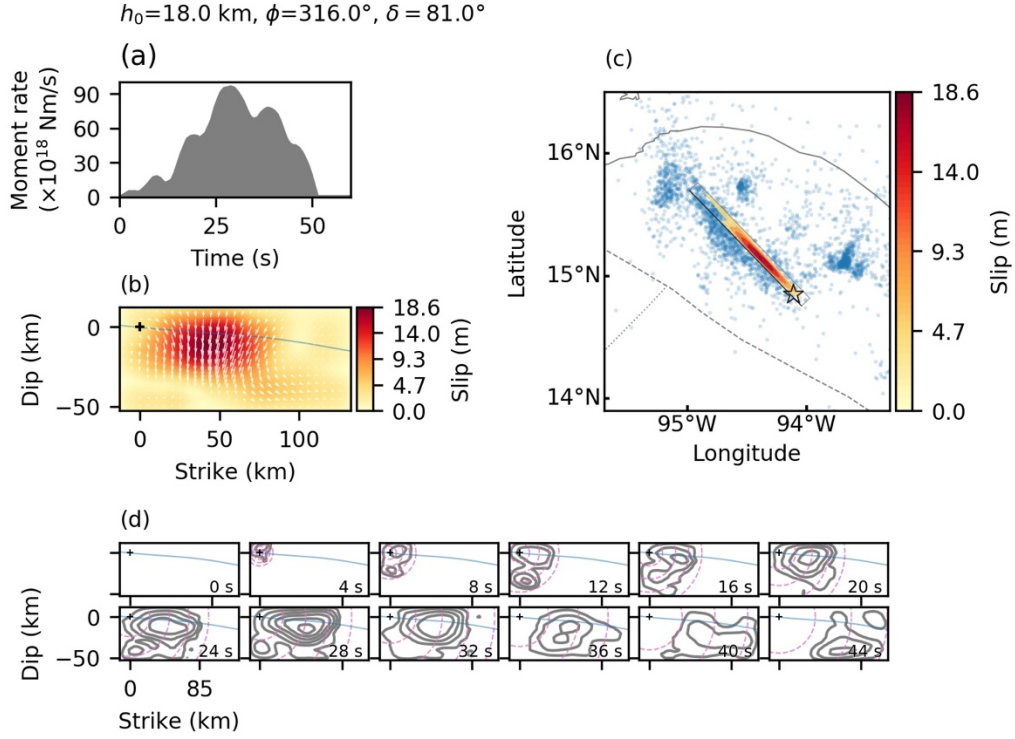
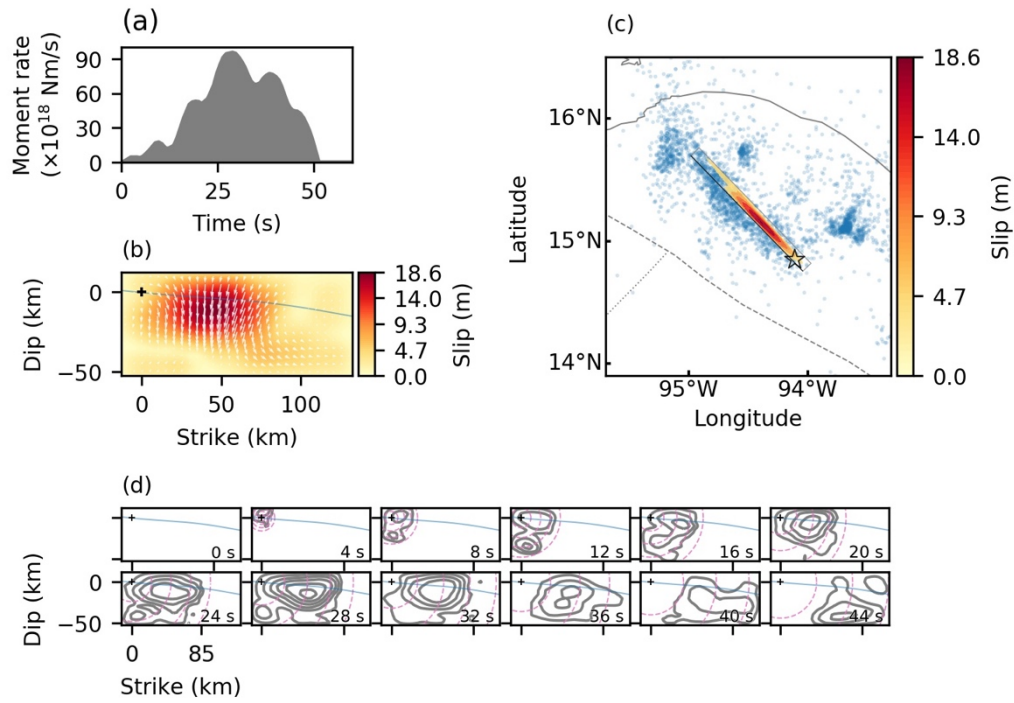


Figure S3. Summary of the slip models with the variable assumptions of dip angle. (a) Graph shows the moment-rate function. The initial rupture depth (h_0), strike angle (ϕ), and dip angle (δ) for the assumed fault geometry are given on left top. (b) Cross section of the cumulative slip distribution. The slip amplitude is represented as color map. White arrows represent the slip vectors of the hanging wall relative to the foot wall. The cross marker is the initial rupture point. (c) Map view of the accumulated slip distribution. Color contour denotes every 3.0 m slip. Rectangle delimits the fault plane along with the fault top as black line. Star and blue dots are the epicenters of the mainshock and the two-week-aftershock ($M \geq 3$) determined by the SSN. (d) Snapshots of the slip model taken. The time where the snapshot is taken is denoted at right-bottom on each panel. Gray contour denotes the slip rate every 0.26 m/s. Cross marker shows the initial rupture point, and blue curve represents the Slab1.0 model (Hayes et al., 2012). Pink dashed lines are the reference rupture speeds that constantly expand in a circle at 1, 2, 3, and 4 km/s.

Near-source velocity model from Santoya et al., 2005 (Table S1)

$$h_0=18.0 \text{ km}, \phi=316.0^\circ, \delta=81.0^\circ$$



Near-source velocity model from Rebollar et al., 1999a (Table S2)

$$h_0=18.0 \text{ km}, \phi=316.0^\circ, \delta=81.0^\circ$$

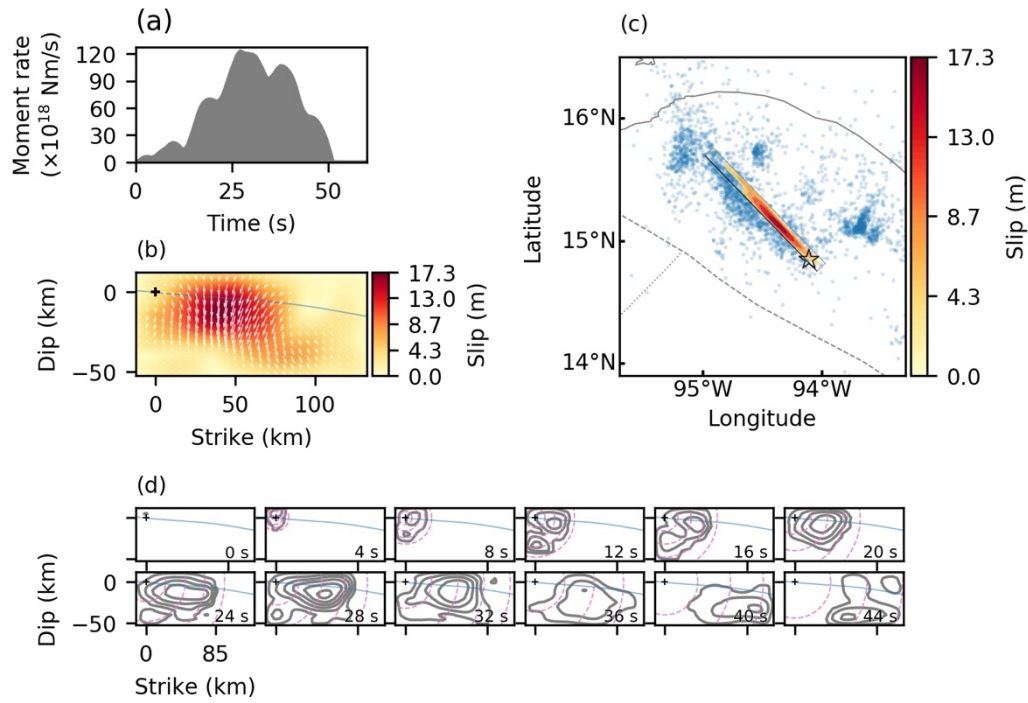


Figure S4. (continued.)

Near-source velocity model from CRUST1.0 (Laske et al., 2013) (Table S3)

$$h_0=18.0 \text{ km}, \phi=316.0^\circ, \delta=81.0^\circ$$

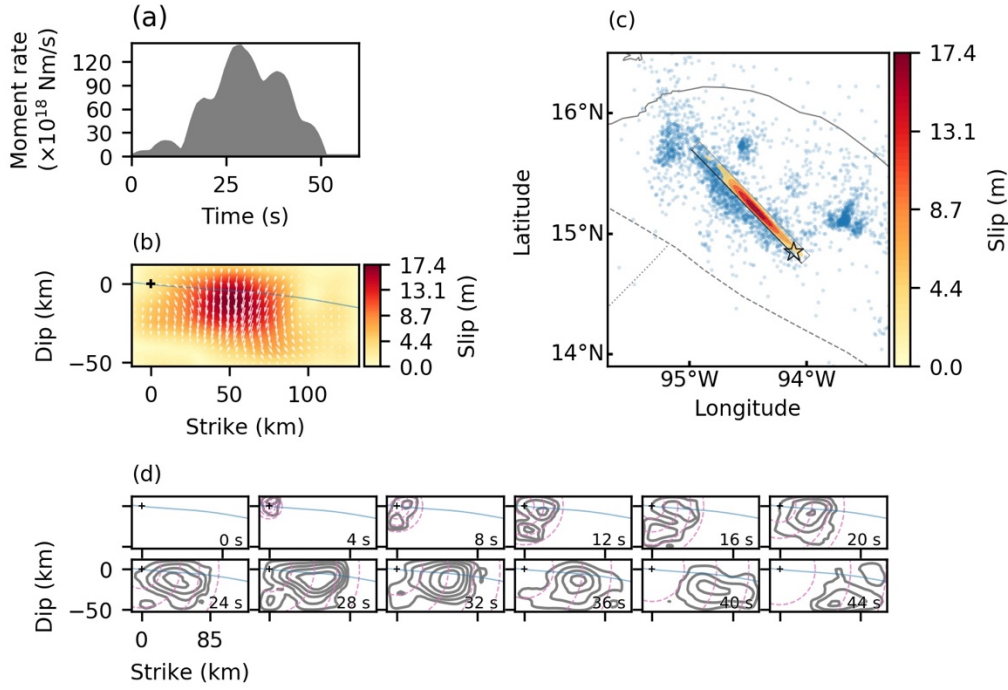


Figure S4. Summary of the slip models based on the different near-source velocity structures. (a) Graph shows the moment-rate function. The initial rupture depth (h_0), strike angle (ϕ), and dip angle (δ) for the assumed fault geometry are given on left top. (b) Cross section of the cumulative slip distribution. The slip amplitude is represented as color map. White arrows represent the slip vectors of the hanging wall relative to the foot wall. The cross marker is the initial rupture point. (c) Map view of the accumulated slip distribution. Color contour denotes every 3.0 m slip. Rectangle delimits the fault plane along with the fault top as black line. Star and blue dots are the epicenters of the mainshock and the two-week-aftershock ($M \geq 3$) determined by the SSN. (d) Snapshots of the slip model taken. The time where the snapshot is taken is denoted at right-bottom on each panel. Gray contour denotes the slip rate every 0.26 m/s. Cross marker shows the initial rupture point, and blue curve represents the Slab1.0 model (Hayes et al., 2012). Pink dashed lines are the reference rupture speeds that constantly expand in a circle at 1, 2, 3, and 4 km/s.



Figure S5. Waveform fittings of the slip models with the variable initial rupture depths presented in Figure 3. Red and gray lines are the normalized synthetic and observed waveforms, respectively. Each trach is aligned by the first arrival of P-phase.

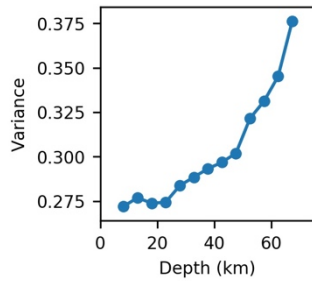


Figure S6. Variance between the observed and synthetic waveforms of the slip models presented in Figure 3, with abscissa for the initial rupture depth.

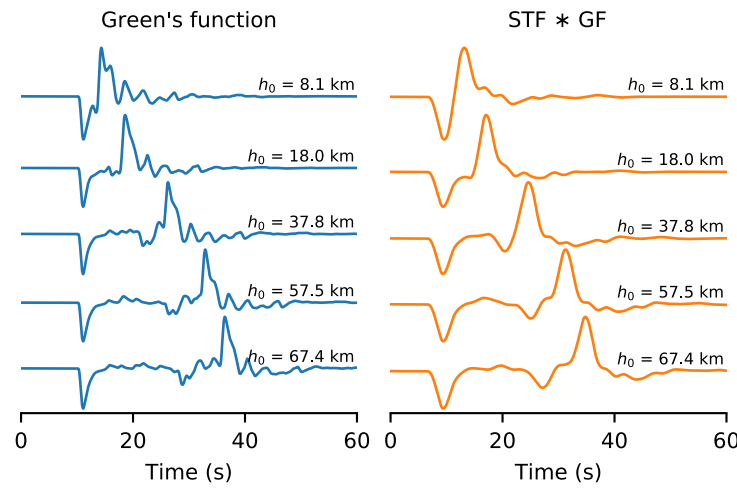


Figure S7. Left panel shows P -wave Green's functions at IU-PTCN station calculated with variable depths (h_0) below the epicenter (14.85°N , 94.11°W) of the 2017 Chiapas earthquake determined by the SSN UNAM with a focal mechanism of {strike, dip, rake} = { 316° , 81° , -85° }, and the right panel shows the convolutions of the GFs and a source time function (STF) composed of triangle function with half duration of 2 s. Each trace is normalized by its maximum amplitude, and the traces are aligned by the onset of P -phase.

V_p (km/s)	V_s (km/s)	Density (10^3 kg/cm 3)	Thickness (km)
1.45	0.00	1.02	1.00
5.30	3.35	2.50	4.00
6.00	3.45	2.76	11.00
6.50	3.80	2.84	20.00
7.40	4.27	2.90	0.00

Table S1. Near-source velocity model used for calculating Green's functions extracted from Santoya et al. (2005).

V_p (km/s)	V_s (km/s)	Density (10^3 kg/cm 3)	Thickness (km)
1.45	0.00	1.02	1.00
5.00	2.89	2.70	4.00
6.20	3.58	2.90	16.00
7.00	4.04	3.00	11.00
7.60	4.39	3.10	12.00
8.20	4.73	3.40	0.00

Table S2. Alternative near-source velocity model used for calculating Green's functions extracted from Rebollar et al. (1999a).

V_p (km/s)	V_s (km/s)	Density (10^3 kg/cm 3)	Thickness (km)
1.50	0.00	1.02	1.00
6.00	3.50	2.72	9.57
6.60	3.80	2.86	6.16
7.10	3.90	3.05	10.27
7.87	4.38	3.25	0.00

Table S3. Alternative near-source velocity model used for calculating Green's functions extracted from CRUST1.0 model (Laske et al., 2013).